LOUIS MONCHICK

MODERN QUANTUM KINETIC THEORY AND SPECTRAL LINE SHAPES

The modern quantum kinetic theory of spectral line shapes is outlined and a typical calculation of a Raman scattered line shape described. The distinguishing feature of this calculation is that it was completely *ab initio* and therefore constituted a test of modern quantum kinetic theory, the state of the art in computing molecular-scattering cross sections, and novel methods of solving kinetic equations. The computation employed a large assortment of tools: group theory, finite-element methods, classic methods of solving coupled sets of ordinary differential equations, graph methods of combining angular momenta, and matrix methods of solving integral equations. Agreement with experimental results was excellent.

THE PROBLEM

Almost with the inception of quantum mechanics, theorists—mostly nuclear and atomic physicists—had developed the general scattering equations necessary to describe collisions between fundamental particles. With almost no exceptions, however, only a few angular momentum and spin states were involved; as a result, these calculations were not computationally intensive. In principle, the general methodology was applicable to the calculation of molecular inelastic and reactive collisions, which are important ingredients of reaction rates, transport properties, and, as in the present case, line broadening. Calculation of these cross sections, however, requires inclusion of many rotation, spin, and orbital angular momentum states as well as several vibrational and electronic states. The number of required states increases linearly and sometimes quadratically with the molecular weight and complexity of the molecules; the result is that problems involving molecular collisions were forced to await the advent of modern computers before they could be attacked. Even then the door had been opened only a chink, because the speed of machines had increased linearly with time, but the size and duration of a computation had increased as the cube of the number of states; therefore, despite the advances in kinetic and scattering theory, only rather approximate methods have been applied to most real problems. These methods, often elegant and ingenious and always plausible, nevertheless had limited applicability and somehow made simplifying assumptions about the fundamental physics of the process.

At present, only systems composed of hydrogen (H_2), deuterium (D_2), and helium (He) can be attacked with a minimum of *ad hoc* assumptions. As a result, these are the only calculations that can be compared directly with experimental results and thus serve as benchmarks for simpler approximations. The calculations presented here will be confined to a He–D_2 system because of the availability of extremely accurate experimental data for comparison,[1] the availability of an extremely good model of the interaction of helium with two deuterium atoms, and the feasibility of carrying out the calculation in a finite time and at a reasonable cost. The goal, which we did not quite reach, was an entirely *ab initio* computation containing assumptions only about the rate of convergence of the numerical procedures used, with no experimental quantities except Planck's and Boltzmann's constants and the electronic charge and mass of the electron, deuteron, and helium nucleus. As described in the following sections, practicality forced us to compromise for an approximation; judging from the outcome, this approximation was quite good. The next section presents a preliminary qualitative description of the theory of line shapes, followed by a brief account of the kinetic theory of line shapes, and then a description of the calculation.

PRELIMINARY REMARKS

Spectra, the interaction of light and matter, have been and still are a major tool for studying electronic structures of atoms and molecules. Loosely speaking, this subject might be characterized as the study of intramolecular forces, because energy levels are determined by a balance between kinetic energy and coulombic interactions. More recently, the realization that collisions influence widths of spectral line shapes has led to the use of spectra to measure intermolecular forces, which are manifested in several contrasting mechanisms that affect the widths and shapes of spectral lines. An isolated atom or a molecule in an excited state is metastable and, if it does not transfer its energy to something else first, radiates its extra energy in the form of a photon. The energy of the photon will not correspond exactly to the difference in energy levels of the excited and ground states, $\Delta E = E_f - E_i \equiv \hbar\omega_{if}$, where $\hbar$ is Planck's constant divided by 2π and ω_{if} is the frequency of the transition, but it will be distributed over a range of ener-

gies. The plot of the intensity of the emitted light versus the energy of the photon, $\hbar\omega$, called the line shape, is more or less a Lorentzian

$$S(\omega) \propto (\omega - \omega_{if} + i\tau^{-1})^{-1} , \quad (1)$$

where τ is the e-folding lifetime of the excited state and ω is the angular frequency. It can be seen that the width, $\Delta\omega = |\omega_{1/2} - \omega_{if}|$, at which the Lorentzian is one-half the maximum, occurs at $\Delta\omega = \tau$, which is just what one would expect from the Heisenberg uncertainty principle. This is called the natural width of a spectral line because, absent any external influences (collisions, fields, measuring apparatus) or motion of the radiating molecule, this width is what would be observed.

In the real world, a molecule is never isolated. It has frequent collisions with other molecules, less frequent ones with the walls, and occasional interactions with externally imposed fields. Consequently, the state, particularly the velocity, of an individual radiating molecule is not known exactly, but it is distributed according to some probability rule, usually taken to be the Maxwell–Boltzmann distribution law

$$f_\alpha^{(0)} = \mathcal{N}^{-1}\exp(-E_\alpha/kT) , \quad (2)$$

where

α is the aggregate quantum number or the set of all the quantum numbers describing all the possible degrees of freedom,
E_α is the energy of this state, including kinetic and thermal,
k is Boltzmann's constant,
T is the absolute temperature,
$f_\alpha^{(0)}$ is the probability of the molecule occupying that state, and
$\mathcal{N}^{-1}$ is a normalization constant.

The kinetic energy component of E_α is mv^2, where m is mass and v is velocity, which means that the radiating molecule is seldom at rest relative to an observer, and therefore every possible value of velocity along the line of sight shifts the frequency of the radiated line by the well-known Doppler shift formula. The center of gravity of each corresponding Lorentzian is shifted as well; thus, the observed line shape must be the resultant of all possible shifted natural line shapes. The result is the familiar Doppler line shape, essentially a Gaussian.

Doppler line shapes are seen only at pressures low enough that the mean time required to complete a radiative transition is reduced to values below the mean time between collisions. At somewhat higher pressures, radiating molecules will collide and change direction several times before the radiation process is completed. Consequently, molecules no longer move in straight lines but execute something like the "drunken man's walk." As a result, even if a molecule does not change its speed, the average velocity along a line of sight, as seen by an observer, decreases, and the line shape narrows and changes shape. This phenomenon, called Dicke narrowing, has been observed many times since it was first predicted.[2]

What has been neglected up to this point is that every collision introduces an uncertainty in the phase of the radiator, which may be reinterpreted as an uncertainty in energy, leading to a widening of the line shape. At high energies and increasing collision frequencies, this effect becomes more important than Dicke narrowing and produces the pressure broadening generally seen at moderate and high pressures. As is well known, the "drunken man's walk" is a diffusion mechanism that measures the average momentum transferred per collision. This value, in turn, is a function of the average component of force along the initial direction of relative motion of two molecules.[3] As an empirical rule of thumb, this process is determined mainly by elastic collisions and the orientation-averaged intermolecular potential. Line broadening, on the other hand, can be a sensitive function of inelastic and reorientating collisions that can occur only if the potential has orientation-dependent components. Observation of a process dependent on the presence of orientation-dependent components is what interests chemical physicists.

THE KINETIC THEORY OF LINE SHAPES

The descriptions in the previous section were confined to an elementary "hand-waving" level and could be refined; but the resulting theory, although easily visualized, would be rather clumsy and jerry-built. The most rigorous way to proceed is to solve the Schrödinger equation or its equivalent, the von Neumann equation, for N interacting molecules and N' photons. The number of interacting molecules, however, is on the order of 10^{23}, which is completely out of the range of feasibility. The popular approach of direct simulation by Monte Carlo methods is also infeasible: even though the number of particles is manageable, 100 to 1000, correlations between gas-phase collisions are negligible, and relevant scattering events are few. It is simpler to use single-particle kinetic equations in which the effects of all possible interactions are accounted for by effective collision cross sections.

Because radiative transitions are functions of the initial and final states and an electromagnetic field, it is natural to use density matrices, ρ^1, the superscript 1 signifying the description of a single representative molecule. The macroscopic value of any classical dynamic variable, A, is then determined by

$$\langle A \rangle = \sum_{ij} \rho_{ij}^1 \mathbf{A}_{ji} \equiv \sum_{ij} \langle \mathrm{i}|\rho^1|\mathrm{j}\rangle \langle \mathrm{j}|\mathbf{A}|\mathrm{i}\rangle = \sum_i \langle \mathrm{i}|\rho^1\mathbf{A}|\mathrm{i}\rangle , \quad (3)$$

where $\mathbf{A}$ is the quantum operator corresponding to A, and $|\mathrm{i}\rangle$ and $\langle \mathrm{j}|$ are the generalized Hilbert-space vectors corresponding to the states i and j. In this representation, ρ_{ij}^1 and $\mathbf{A}_{ji}$ are seen to be the quantum analogs of a classical

distribution function and a classical dynamic variable. Indeed, the diagonal element of ρ^1, ρ^1_{ij} can be identified as the population density of the ith quantum state. The off-diagonal elements, ρ^1_{ij}, $i \neq j$, which vary with time as $\exp[i\hbar^{-1}(E_i - E_j)t]$ in the absence of any interaction, are interference terms. In the presence of an external field, they have the added significance of being a measure of the polarization induced by the field.

Another characteristic of singlet-density matrices is that, because they describe single, representative molecules, all information concerning fluctuations is lost. This characteristic is not a drawback as regards line shapes, however, because they are directly related to the spectral response function, which in turn is related to $\tilde{\rho}$, a Laplace transform of ρ,

$$S(\omega) = \sum \langle \mathbf{i}|\mathrm{P}^{\dagger}\tilde{\rho}\ \mathrm{P}|\,\mathbf{j}\,\rangle\,, \tag{4}$$

$$\tilde{\rho} \equiv \int \exp(\iota\omega t + \iota k\cdot x)\rho\ dt\ d^3x\ . \tag{5}$$

Here P and its adjoint, $\mathrm{P}^{\dagger}$, are the operator equivalents of the polarization of the radiating molecule induced by an electromagnetic field. In the presence of a weak or moderate-strength electromagnetic field, the density matrix obeys the following equation if the translational degrees of freedom can be treated classically[4] as

$$\iota(\omega - \omega_{if} + \mathbf{k}\cdot\mathbf{x})\tilde{\rho}_{\mathrm{D}_2} + (\mathbf{T}\tilde{\rho}_{\mathrm{D}_2}) = f^{(0)}_{\mathrm{D}_2}\rho\ , \tag{6}$$

where $(\mathbf{T}\tilde{\rho}^{(2)})$ is a shorthand notation of the average sum of all the interactions of the other $N - 1$ molecules with the Nth, and $\tilde{\rho}^{(2)}$ is the density matrix of a pair of molecules obtained by fixing their quantum state and averaging and summing over the states of the remaining $N - 2$ molecules. Thus defined, $\tilde{\rho}^{(2)}$ is a complex functional of $\tilde{\rho}^{(1)}$, $(\mathbf{T}\tilde{\rho}^{(2)})$ is a complex functional of $\tilde{\rho}^{(2)}$, and the reduced kinetic equation is in principle exact even though fluctuation phenomena are buried deep inside $(\mathbf{T}\tilde{\rho}^{(2)})$.

In actuality, however, the exact form of $(\mathbf{T}\tilde{\rho}^{(2)})$ is not known, and we have to use a set of approximations that, although for the most part supply a very good description of dilute gases, have not gone unchallenged. These approximations are as follows: (1) the interaction between the two molecules is described from knowledge of the results of completed collisions that occur on a time scale that is much smaller than that of any other process in the gas; (2) before a collision, or sets of collisions, the states of two molecules are totally uncorrelated; and (3) only first-order corrections need be retained for deviations from local equilibrium. The first assumption is known to violate detailed balance in the theory of spectra of overlapping lines and to yield poor descriptions of the far wings of broad spectral lines because the spectral response function depends directly on the difference of the radiation field frequency and the natural resonant frequency of the line. According to the Heisenberg uncertainty principle, the uncertainty in the radiative lifetime varies inversely with this frequency difference; thus, the duration of a collision cannot be considered negligible far out in the wings of a spectral line. These reservations can be waived in the present case, which concerns very narrow, exactly resonant, isolated lines. The second approximation is Boltzmann's *stosszahlansatz*, which has been violated by many computer experiments designed to simulate dense gases and liquids, but which, it seems, can be safely ignored at low and moderate pressures. The third is well satisfied by the experiment considered here.

The rather complex term $\mathbf{T}\tilde{\rho}^{(2)}$ has been written as the result of operating on a density matrix $\tilde{\rho}^{(2)}$ with a "superoperator" or tetradic $\mathbf{T}$; both terms are common usage. The first approximation allows us to write $\mathbf{T}\tilde{\rho}^{(2)}$ in a form that slightly resembles the familiar Boltzmann collision operator:[5,6]

$$\mathbf{T}\tilde{\rho}^{(2)} = -(2\pi)^4\hbar^2 \int d^3\mathbf{p}_{\mathrm{He}} \left[\int d^3\mathbf{p}_{\mathrm{D}_2} \int d^3\mathbf{p}'_{\mathrm{He}} \times t\tilde{\rho}^{(2)}t^{\dagger} + \frac{1}{2\pi}\,(t\tilde{\rho}^{(2)} - \tilde{\rho}^{(2)}t^{\dagger})\right]\ . \tag{7}$$

Here t, which will be discussed briefly in the next section, is the familiar t-matrix of scattering theory; $t^{\dagger}$ is its adjoint; and $t\tilde{\rho}^{(2)}t^{\dagger}$, $t\tilde{\rho}^{(2)}$, and $\tilde{\rho}^{(2)}t^{\dagger}$ are matrix products. All integrations and implied sums are understood to be confined to the energy shell, that is, those collisions where energy is conserved. The second and third approximations allow us to replace $\tilde{\rho}^{(2)}$ by $\tilde{\rho}_{D_2} f^{(0)}_{\mathrm{He}}$.

Here we have implicitly assumed that the He concentration is so much larger than the D_2 concentration that the He is always in equilibrium; this equilibrium reduces the dissimilarity somewhat between $\mathbf{T}\tilde{\rho}$ and the Boltzmann collision operator, but the kinetic equation still retains t-matrices rather than cross sections as a necessary component because of the possibility of interference patterns set up after every collision. The initial wave packet, essentially a partially localized plain wave, is broken up into a set of scattered waves corresponding to the set of final states populated by the collision. The vibrational and electronic energy levels usually are sufficiently well separated to allow scattered waves to separate in space before the next collision and not mutually interfere (Fig. 1). Nearly degenerate states, such as those that occur in rotation multiplets and electronic fine structure, usually cannot separate as well as those shown in the figure, resulting in interferences.

Equation 7 shows that, because $\tilde{\rho}_{\mathrm{D}_2}$ is not known exactly but only implicitly as the solution of a rather complicated equation, it will be a rather complex function of all the translational and internal degrees of freedom. As in the case of the Boltzmann equation, $\tilde{\rho}$ may be simplified slightly because of several constraints that $\mathbf{T}$ must satisfy in all stages of approximation. One is that $\mathbf{T}$ be independent of the frame of reference; in particular, it

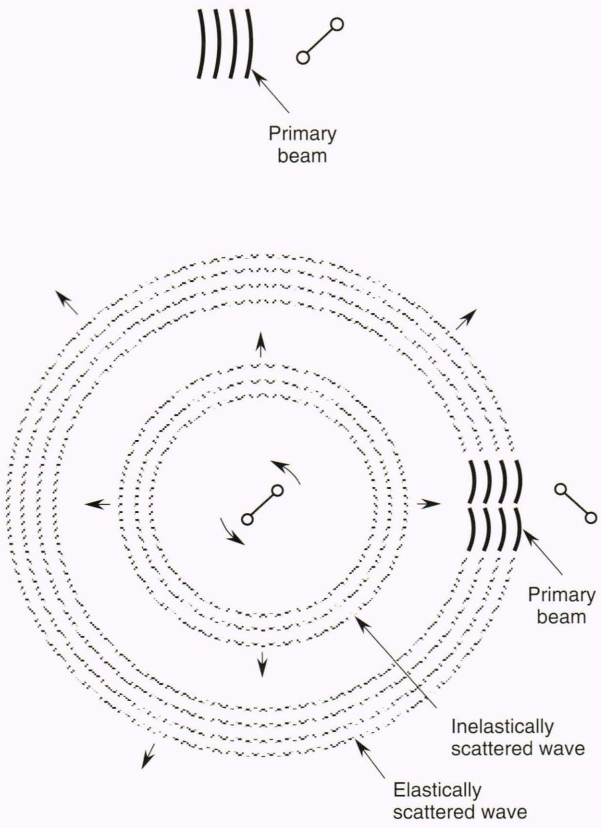

Figure 1. A wave packet approaches a target, in this example (top), a diatomic molecule. A short time after the collision (bottom), the primary beam, slightly attenuated, is on the verge of colliding with another molecule. Elastically scattered waves are radiating outward with the same relative velocity as the primary beam and have moved the same distance from the target. Inelastically scattered waves have moved away at a slower speed and are well separated from the elastically scattered waves.

should be rotationally invariant. It is then natural to expand $\tilde{\rho}_{D_2}$ in an infinite series of density matrices minimally affected by the orientation of the gas relative to an observer. These matrices are chosen to be the irreducible representations of the rotation group, $U^{JM}_{j_i j_f q L}(\hat{v})$, which have the property that all matrices with a given value of J and M transform under rotations into linear sums of the other matrices with the same value of J and M, and no others.[7] Then ρ can be expanded as

$$\tilde{\rho}_{D_2} = \sum_{J,M,L,q} \tilde{\rho}^{JM}_{j_i j_f q L}(v)\ U^{JM}_{j_i j_f q L}(\hat{v}) . \qquad (8)$$

The eigenfunctions, U, are really operators and must couple rotation eigenfunctions of the translational momentum, $Y^L_m(\hat{v})$, to the rotational angular momentum of the states before and after the radiative transition; q is the magnitude of the pseudo-angular momentum resultant of $|j_i m_i\rangle$ and $\langle j_f m_f|$, and J is the resultant of adding the momenta L and q. By the usual quantization rules, the allowed values of q and J are restricted to

$$|j_i - j_f| \le q \le j_i + j_f$$

$$|q - L| \le J \le q + L .$$

Because of the rotational invariance of $\mathbf{T}$, this choice of expansion has the desirable consequence that all tetradics of $\mathbf{T}$ and other rotationally invariant superoperators are block diagonal in J and M. In mathematical notation,

$$\langle\langle U^{JM}_{j_i j_f q L}(\hat{v})\ |\mathbf{T}|\ U^{J'M'}_{j_i' j_f' q' L'}(\hat{v})\rangle\rangle = 0 ,$$

$$J \neq J',\ M \neq M' . \qquad (9)$$

This is shown schematically in Figure 2, specifically,

$$\mathbf{T}\tilde{\rho}_{D_2} = \sum_{JM} \sum_{j_i j_f} \sum_{qL} \sum_{j_i' j_f'} \sum_{q'L'} U^{JM}_{j_i j_f q L}(\hat{v}) \times \int_0^\infty K^J(j_i j_f q L v; j_i' j_f' q' L' v') \times \tilde{\rho}^{JM}_{j_i' j_f' q' L'}(v') v'^2 dv' . \qquad (10)$$

As shown in Equation 10, other desirable dividends of this elementary application of group theory are as follows: (1) the kernel and the expansion coefficient under the integral sign are now scalars; (2) the integration over velocity orientations has been buried in the kernel; and (3) the kernel itself is a symmetric function of the dynamic variables before the collision, which are represented by the primed quantities, and the postcollision variables, which are represented by the unprimed quantities. The last feature now allows us to employ any of the battery of methods developed for integral equations with symmetric kernels.[8]

Tangent to the blocks diagonal in J (Fig. 2) are two parallel diagonal rows that result from the coupling of the J, $J \pm 1$ blocks by the drift terms in the quantum Boltzmann equation. This comes about because, although the collision terms are independent of the placement of an observer, the presence of an electromagnetic field defines a preferred direction that enters into the drift terms. At the higher densities, the collision terms—represented by the diagonal blocks—dominate, and the Y^0_0 component of the density matrix is effectively decoupled from the higher-order nonspherical terms. The line shape is then determined by the pressure-broadening cross section and assumes the familiar Lorentzian shape. At progressively lower densities, however, the drift terms become more important, and more and more nonspherical terms are coupled by the kinetic equation, affecting the spherical term to at least second order. The most important of these are the $Y^{0,\pm 1}_1$ tensorial components. The matrix element of the collision operator sandwiched by

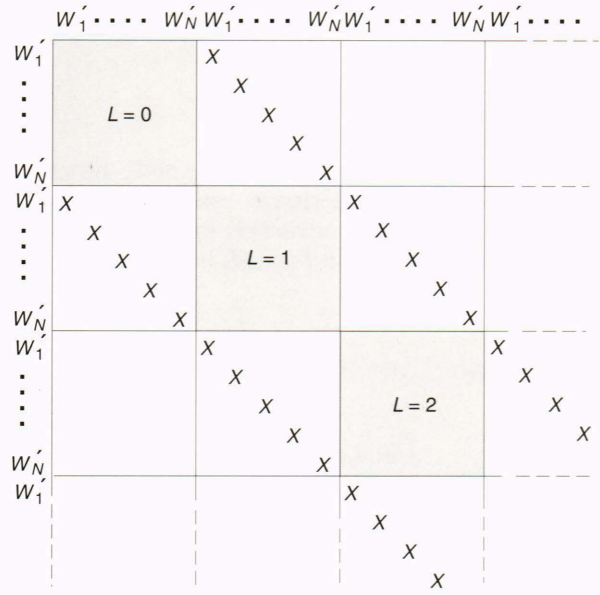

Figure 2. The matrix of the collision kernel $K^L(W_i, W_j')$, where the velocity distribution function has been expanded in spherical harmonics $Y_M^L(\hat{v})$, and W_i is the postcollision and W_j' the precollision values of the (normalized) velocity evaluated at the pivot points of a suitably chosen Gaussian integration algorithm. Each *X* corresponds to a nonvanishing matrix element.

these components is the momentum transfer cross section, long familiar to the kinetic theory of diffusion. The line width, which is dominated by the relaxation term at high densities, decreases as the density is decreased until the diffusion terms, which vary inversely with the density, assume the dominant role and the line width increases again, eventually approaching the Doppler line shape at very low pressures.

THE COMPUTATION

Several years ago, scientists at the National Institute of Standards and Technology[1] began extremely accurate measurements of Raman scattering of D_2 in several gases, including He. These experiments measured the polarized Stokes–Raman Q-branch ($\Delta j = 0$) scattering of frequencies corresponding to the $v = 0 \rightarrow 1$ vibrational transition of D_2 at densities ranging from a fraction of an Amagat to 8 Amagats. An Amagat is a unit of density and volume defined as the ratio of the number of molecules per cubic centimeter to the number of molecules per cubic centimeter in a perfect gas at 1 atmosphere of pressure and at 0° C. In coherent anti-Stokes–Raman scattering a laser beam is formed with a multiple of some frequency approximating the separation of two quantum levels of a chosen molecule. The sample is irradiated with this beam and a probing beam with a different tunable frequency. Spectral transitions are now induced; this is called scattering because photons are taken out of the primary beam. If the transition is to a higher level, this is called anti-Stokes scattering. If the initial and final rotational states are the same, this is called a Q-branch transition.

This set of experimental conditions included line shapes dominated by the Dicke narrowing as well as those characterized by high-pressure broadening. At the same time, Robert Blackmore (a postdoctoral fellow at APL), Sheldon Green (a scientist at NASA), and I undertook a calculation of these effects in D_2 immersed in He, making a minimal number of extraneous physical assumptions. This calculation required (1) ascertaining the intermolecular forces between D_2 and He, (2) solving the scattering equations for all events relevant to line-shape broadening, and (3) inserting the resulting cross sections into the appropriate kinetic theory and solving for the spectral response function, which produces the line shape.

A glance at the collision kernels describing classic structureless particles shows that they are not simple. The quantum version is even more complex. For as simple a system as D_2–He, as many as eight angular momenta are coupled in the final complex formula for the collision kernels, $K^j(j_i j_f qLv; j_i' j_f' q'L'v')$. The first step is the computation of matrix elements of the D_2–He potential energy for a small set of rotational and vibrational states; the second step is the solution of the scattering equations for the t-matrices; the third step is the insertion of these t-matrices into collision kernels; and the fourth step is the solution of the quantum kinetic equation.

Some years ago, a molecular orbital calculation was carried out for the electronic energy of two hydrogen-like atoms and a helium atom clamped in space at several configurations.[9] For this clamped potential energy surface, $\tilde{V}(|r|, |R|, r \cdot R)$, which is known as the Meyer–Hariharan–Kutzelnigg potential, $|r|$ is the distance between D_2 and He, $|R|$ is the D–D internuclear distance, and $r \cdot R$ is a measure of the relative orientation of D_2 and He. The potential energy surface is also valid for two D atoms and one He atom clamped in space. The accuracy of this surface is borne out by many comparisons of experiment and predictions based on it. At each D_2–He separation and relative orientation, the potential energy surface was calculated at five D–D separations. It is now convenient to replace the R-dependent potential energy surface, $\tilde{V}$, by the vibrational matrix elements of $\tilde{V}$, that is, by a set of integrals of $\tilde{V}$ sandwiched by the initial and final vibrational state. The method chosen to solve the wave equation for the relative nuclear motion was, by interpolation in the variable R, to evaluate V at the pivot points of a suitable Hermite polynomial. This procedure is similar in spirit to the pseudospectral methods described by Ku and Rosenberg in this issue. The differential equation in R could then be converted to a matrix equation, which was then solved with the usual normalization and boundary conditions. When the vibrational energy eigenvalues calculated at large D_2–He separations were compared with spectroscopic values, accuracies of $\approx 0.2\%$ were indicated for the vibrational wave functions, $\chi_v(|R|)$. Most of the calculations of vibrational–rotational matrix elements,

$$\int dR\, [\chi_{v'}(|R|) Y_{m'}^{j'}(\hat{R})]^* \tilde{V}(|r|, |R|, r \cdot R) \chi_v(|R|) Y_m^j(\hat{R}) , \quad (11)$$

were carried out with rigid rotor rotational wave functions, $Y_m^j(\hat{R})$, with rotational energies corrected for centrifugal stretching. A final set also included centrifugal stretching in the vibrational wave function. The vibrational and rotational quantum numbers included were $v = 0, 1$ and $j = 0, 1, 2, 3, 4, 5, 6, 7$. These calculations were carried out in overnight runs on an IBM AT, and the potential energy matrices were then sent via BITNET to New York for step two.

Because this is a quantum mechanical system, the scattering information is obtained not from trajectories but from solving the Schrödinger equation with the solutions having the asymptotic form

$$\exp(\iota k \cdot r) X_v(|R|) Y_m^j(\hat{R})$$

$$- \sum_{v'j'm'} 2\pi\iota r^{-1} \exp(\iota |k'||r|) t_{vjm,v'j'm'} X_{v'}(|R|) Y_{n'}^{j'}(\hat{R}) \; . \tag{12}$$

The usual practice in molecular-scattering calculations is to expand a prototype wave function in the set of all possible internal states—and a few closed channels as well—and a large number of partial waves representing the resultant of the rotational and orbital angular momenta of the trajectories of relative motion. This representation is chosen because scattering equations are rotationally invariant in the relative motion frame of reference and become block diagonal if the expansion set is taken to be the set of total angular momentum eigenfunctions. The required number is established by making a few test calculations to determine the rate of convergence. The time-independent Schrödinger equation is then solved at a single total energy for all possible independent boundary conditions, and the solutions are then combined into wave functions having the asymptotic form of Equation 12. The requisite scattering information is determined by the asymptotic value of the wave function at the completion of the collision and succinctly represented by the contracted set of data composed of the t-matrices. The t-matrices represent the contracted set. These data are calculated automatically by a software package called MOLSCAT,[10] which requires as input only the potential energy matrices calculated in step one. The scattering information was destined for a Q ($\Delta j = 0$) branch $v = 0 \rightarrow 1$ Raman line, requiring calculations for $v = 0$ and for $v = 1$. The required calculations were performed on a NASA IBM 360 during several overnight runs, and the results were returned to APL on tape.

In step three, the t-matrices were recoupled to form the collision kernels. This step was necessary because the scattering matrices and the collision kernels are rotationally invariant in different spaces. Development of a formula for the collision kernels was not a straightforward task,[7] but rather depended on choosing a momentum space transformation that is not at all obvious. One final approximation was introduced that set $q = 0$ and reduced the size of the computation. The subsequent coding of the resultant formula for the computer was laborious but straightforward. In line broadening, the coding involved summing products of two t-matrices and terms representing all the possible couplings of the magnitudes of six angular momenta. No chains of interior matrix multiplications could be optimized other than the sums over magnetic quantum numbers that already had been carried out analytically and were now buried inside the coupling coefficients, which are known in the trade as 6-J symbols. The code was optimized somewhat by evaluating the 6-J symbols recursively, but even then a typical calculation took between thirty minutes and two hours on the Ahmdahl 5890-200E.

In the final stage, the kernels were evaluated at the pivot points of a Laguerre polynomial of order $N = 30$, converting the integrals over v' in Equation 10 into a 30×30 matrix multiplying a vector of order 30. As is well known, this conversion is equivalent to approximating the density-matrix coefficients with an expansion in Laguerre polynomials truncated at the 30th term. In principle, the density matrix could have been expanded directly in Laguerre polynomials, and each of the matrix elements could have been evaluated individually as in the older texts on kinetic theory. The present procedure avoids that step by doing it automatically. Remembering that, with the last approximation, $J = L$, Equation 6 could then be mapped onto a matrix equation

$$A \cdot x = y \; .$$

Matrix A is composed of 30×30 blocks clustered along the diagonal with the blocks ordered by increasing values of J. As noted in the previous section, the blocks are coupled by two parallels to the diagonal (cf. Fig. 2), which become increasingly important at lower densities. Preliminary calculations indicated that including J-blocks up to $J = 5$ was sufficient to represent the spherical part of the density matrix near the Dicke narrowing minimum (Fig. 3). The final computation then proceed-

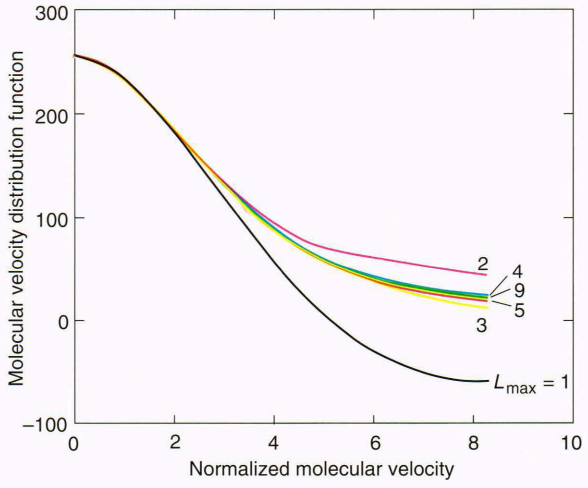

Figure 3. The deviation of the $L = 0$ component of the density matrix, ρ, from a Maxwell–Boltzmann distribution as a function of a normalized velocity and of the maximum value of L when ρ is expanded in a series of spherical harmonics, $Y_M^L(\hat{v})$.

ed by inverting the 180 × 180 sparse matrix at a series of densities and frequencies. This relatively small calculation could be done overnight on a 386 PC.

RESULTS

The experimental results to be reproduced were obtained by first forming a sharply focused, almost monochromatic laser beam corresponding to the $\Delta j = 0, \Delta v = 0 \rightarrow 1$ transition of D_2. The beam entered a cell containing a 90% He:10% D_2 mixture and traversed it about forty times. The values that we have called "experimental" have been corrected for backward scattering and interferences that occur each time a ray traversing the cell crosses another ray. The measured line shapes were then attributed to Raman scattering in the forward direction, and the line widths and shifts were calculated from phenomenological formula fit to the measurements.

In the calculations reported here, the frequency grid was fine enough to allow evaluation of the widths and shifts directly from the numerical results. The high-density widths and shifts vary almost linearly with density. The asymptotic density coefficients of these quantities are shown in Table 1.[11] Computations incorporating centrifugal stretching and vibrationally inelastic effects do not cause any significant improvement. Considering the availability of only five points with which to evaluate vibrational wave functions and the fact that width and shift coefficients are evaluated by the asymptotic variation, the agreement with experimental results is about as good as can be expected.

A representative set of line shapes[8] at a given value of j_{rot} (i.e., the rotational quantum number) is shown in Figure 4. Line widths as a function of density and j_{rot} are shown in Figures 5 to 7 for both computed and experimental results. The difference between the two is due in part to differences in the numerical methods used for extracting half-widths from the raw experimental data and computed line-shape data. Detailed comparison of calculated and experimental line shapes shows few discernible differences.[12] All in all, the results were very gratifying.

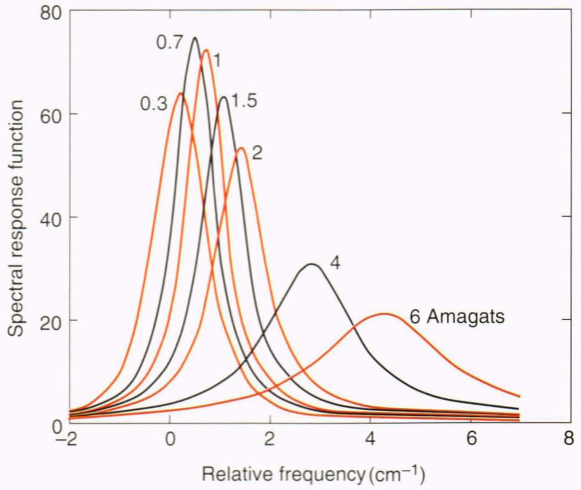

Figure 4. The spectral response function for $j_{rot} = 0$ evaluated at a set of densities ranging from 0.3 to 6 Amagats. At 6 Amagats, the spectral response function is almost Lorentzian. (An Amagat is a unit of volume and density defined as the ratio of the number of molecules per cubic centimeter to the number of molecules per cubic centimeter in a perfect gas at 1 atmosphere of pressure and at 0° C; j_{rot} is the rotational quantum number.)

The achievements of this study can be summarized as follows:

1. The accuracy of the Meyer–Hariharan–Kutzelnigg He–H_2 potential energy surface was demonstrated once again.

Table 1. Comparison of theoretical and experimental width and shift parameters for the $Q(J)$ lines of D_2 in He at 298 K.

	Width					Shift	
J	Experiment[a]	Theory	y^0_{in}	y^1_{in}	y_{dep}	Experiment[b]	Theory
0	2.35	2.33	0.73	1.00	0.60	6.1	7.2
1	1.20	1.11	0.18	0.24	0.69	6.5	7.7
2	1.73	1.66	0.40	0.54	0.72	6.8	7.7
3	1.62	1.54	0.34	0.45	0.75	6.9	7.9
4	1.40	1.29	0.22	0.29	0.78	6.8	8.0
5	1.20	1.14	0.16	0.23	0.82	NM	8.2

Note: Theoretical values include centrifugal distortion in the potential matrix elements but not in the rotational energy levels; vibrational inelasticity is ignored. The theoretical widths have been decomposed into the dephasing part, y_{dep}, and the inelastic contributions within $v = 0$ and $v = 1$, y^0_{in} and y^1_{in}, respectively. All values are in 10^{-3} cm^{-1}/Amagat. NM = not measured.

[a]Reprinted, with permission, from Ref. 1.

[b]G. J. Rosasco and W. Hurst, personal communication, 1989.

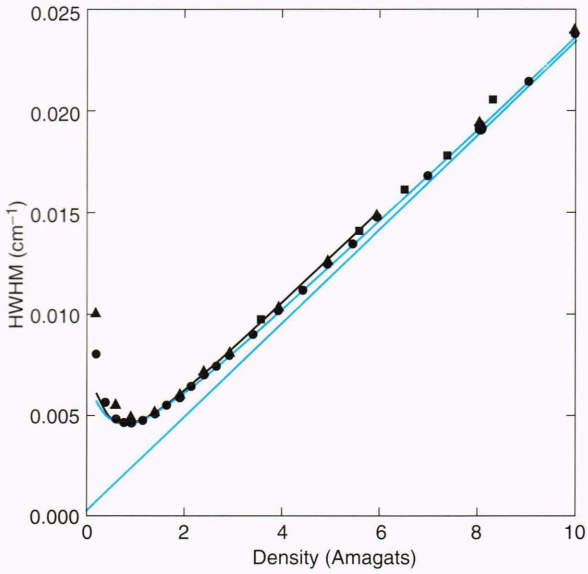

Figure 5. The half-width at half-maximum (HWHM) of the spectral response curve for the Stokes–Raman Q-branch scattering of the $v = 0 \rightarrow 1$ transition of D_2 immersed in helium: $j_{rot} = 0$ (j_{rot} is the rotational quantum number). The squares are experimental data. The solid black line is the curve predicted by the calculation described here. The circles are the results of a slightly amplified calculation; the other symbols and colored lines are the results of more approximate theories.

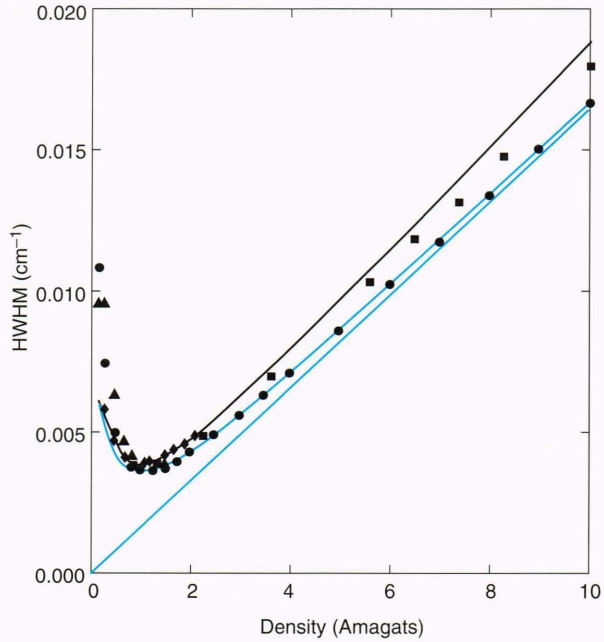

Figure 7. The half-width at half-maximum (HWHM) of the spectral response curve for the Stokes–Raman Q-branch scattering of the $v = 0 \rightarrow 1$ transition of D_2 immersed in helium: $j_{rot} = 2$ (j_{rot} is the rotational quantum number). The notation is the same as in Figure 5.

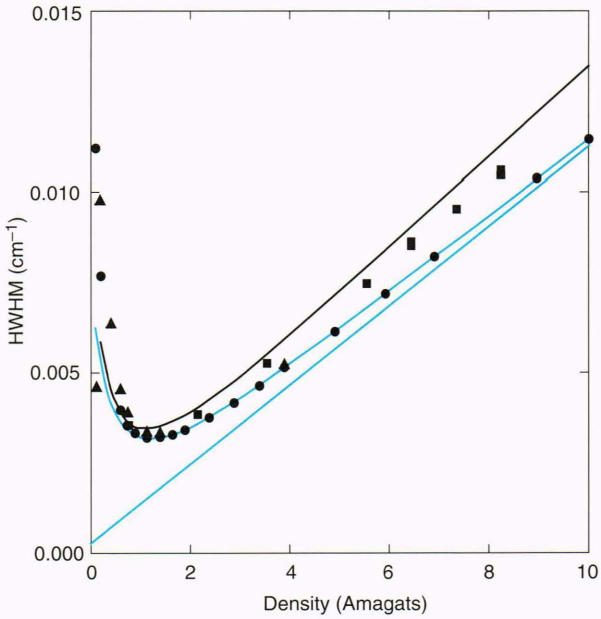

Figure 6. The half-width at half-maximum (HWHM) of the spectral response curve for the Stokes–Raman Q-branch scattering of the $v = 0 \rightarrow 1$ transition of D_2 immersed in helium: $j_{rot} = 1$ (j_{rot} is the rotational quantum number). The notation is the same as in Figure 5.

2. Modern molecular-scattering methods have progressed to the point where they are, in principle, applicable to all molecular and kinetic processes.

3. Generalized quantum kinetic equations can be solved by collision kernel methods, otherwise known as discrete ordinate methods, that had been developed for neutron diffusion and planetary escape processes, effecting a significant improvement in computational speed and accuracy. A drawback is that the results are not represented by a simple formula.

4. In principle, extensions to higher-order tensor polarizations can be made by using sparse matrix and perturbation methods.

5. In each of the preceding conclusions, the qualifying phrase "in principle" means "provided enough computational power is in hand."

These calculations may be considered a validation of the current state-of-the-art molecular scattering theory and gas kinetic theory. Although not described here, these calculations also served as benchmarks for simpler, more approximate methods. The latter are now being applied to deuterium/hydrogen rotational transitions in the upper atmospheres of the outer planets (J. Schaefer and L. Monchick, unpublished data). One immediate application is the estimation of the deuterium/hydrogen concentration in the atmospheres of Jupiter, Neptune, and Saturn.[13]

REFERENCES

[1] Smyth, K. C., Rosasco, G. J., and Hurst, W. E., "Measurement and Rate Law Analysis of D_2 Q-Branch Line Broadening Coefficients for Collisions with D_2, He, Ar, H_2, and CH_4," *J. Chem. Phys.* **87**, 1001–1011 (1987).

[2] Dicke, R. H., "The Effect of Collisions upon the Doppler Width of Spectral Lines," *Phys. Rev.* **89**, 472–473 (1953).

[3] Monchick, L., "The Ehrenfest Theorem and Gas Transport Properties," *Physica* **78**, 64–78 (1974).

[4] Hess, S., "Kinetic Theory of Spectral Line Shapes. The Transition Between Doppler Broadening and Collisional Broadening," *Physica* **61**, 80–94 (1972).
[5] Monchick, L., and Hunter, L. W., "Diatomic-Diatomic Molecular Collision Integrals for Pressure Broadening and Dicke Narrowing: A Generalization of Hess's Theory," *J. Chem. Phys.* **85**, 713–718 (1986).
[6] Tip, A., "Transport Equations for Dilute Gases with Internal Degrees of Freedom," *Physica* **52**, 493–522 (1971).
[7] Blackmore, R., "Collision Kernels for the Waldmann–Snider Equation," *J. Chem. Phys.* **86**, 4188–4197 (1987).
[8] Blackmore, R. J., Green, S., and Monchick, L., "Dicke Narrowing of the Polarized Stokes–Raman Q Branch of the $\nu = 0 \rightarrow 1$ Transition of D_2 in He," *J. Chem. Phys.* **91**, 3846–3853 (1989).
[9] Meyer, W., Hariharan, P. C., and Kutzelnigg, W., "Refined *ab initio* Calculations of the Potential Energy Surface of He–H_2 with Special Emphasis on the Region of the van der Waals Minimum," *J. Chem. Phys.* **73**, 1880–1897 (1980).
[10] Hutson, J. M., and Green, S., *MOLSCAT Computational Code, Version 9*, Collaborative Computational Project No. 6, Science and Engineering Research Council, Cambridge, U.K. (1986).
[11] Green, S., Blackmore, R., and Monchick, L., "Comment on Line Widths and Shifts in the Stokes–Raman Q Branch of D_2 in He," *J. Chem. Phys.* **91**, 52–55 (1989).
[12] Rosasco, G. J., Bowers, W. J., Hurst, W. S., Smyth, K. C., and May, A. D., "Simultaneous Forward-Backward Raman Scattering Studies of D_2:X (X = D_2, He, Ar)," *J. Chem. Phys.* **94**, 7625–7633 (1991).
[13] Bezard, B., Gautier, D., and Marten, A., "Detectability of HD and Non-Equilibrium Species in the Upper Atmospheres of the Giant Planets from Their Submillimeter Spectrum," *Astron. Astrophys.* **161**, 387–411 (1986).

THE AUTHOR

LOUIS MONCHICK was born in Brooklyn, New York, grew up in a suburb of Boston, and received his A.B., M.S., and Ph.D. degrees from Boston University, the Ph.D. in 1954. After brief stays at the University of Notre Dame and General Electric, he came to APL in July 1957. Except for several visits to the JHU Homewood campus as part-time assistant professor and Parsons Professor, and to the Universities of Bielefeld and Leiden as a visiting scientist, he has remained at APL. Dr. Monchick has worked in the fields of diffusion-controlled reactions, molecular collision dynamics, and transport properties of polyatomic gases. Two publications in the last field made the "twenty-two most cited" list of articles published by APL staff members (Berl, W. G., *Johns Hopkins APL Tech. Dig.*, Vol. 7, No. 3, 221, 1986). One of these papers was also given the award of "Citation Classic" by *Current Contents*.